Stem cell and tissue regeneration analysis in low-dose irradiated planarians treated with cerium oxide nanoparticles

Stem-cell and tissue-regeneration analysis in low-dose irradiated planarians treated with cerium oxide nanoparticles

Alessandra Salvetti[1*], Gaetana Gambino[1], Leonardo Rossi[1], Daniele De Pasquale[2,3], Carlotta Pucci[2], Stefania Linsalata[4], Andrea Degl'Innocenti[2], Simone Nitti[5], Mirko Prato[6], Chiara Ippolito[7], Gianni Ciofani[2*]

1 Università di Pisa, Dipartimento di Medicina Clinica e Sperimentale, Via Alessandro Volta 4, 56126 Pisa, Italy

2 Istituto Italiano di Tecnologia, Smart Bio-Interfaces, Viale Rinaldo Piaggio 34, 56025 Pontedera, Italy

3 Scuola Superiore Sant'Anna, The Biorobotics Institute, Smart Bio-Interfaces, Viale Rinaldo Piaggio 34, 56025 Pontedera, Italy

4 Azienda Ospedaliero Universitaria Pisana, Via Roma 67, 56126 Pisa, Italy

5 Istituto Italiano di Tecnologia, NanoChemistry, Via Morego 30, 16163 Genova, Italy

6 Istituto Italiano di Tecnologia, Materials Characterization Facility, Via Morego 30, 16163 Genova, Italy

7 Università di Pisa, Dipartimento di Medicina Clinica e Sperimentale, Via Roma 55, 56126 Pisa, Italy

* Corresponding authors: Gianni Ciofani gianni.ciofani@iit.it; Alessandra Salvetti alessandra.salvetti@unipi.it

The authors declare that they have no conflict of interests.

Abstract

Owing to the self-renewing reactive oxygen species (ROS) scavenger capability of cerium oxide nanoparticles (nanoceria), we tested *in vivo* radioprotective effects on stem cells and tissue regeneration using low-dose irradiated planarians as model system. We treated planarians with nanoceria or gum Arabic, as control, and we analyzed the expression of stem-cell molecular markers and tissue-regeneration capability, as well as cell death and DNA damage in non-irradiated and in low-dose irradiated animals. Our findings show that nanoceria increase the number of stem cells and tissue regenerative capability, and reduce cell death and DNA damage after low-dose irradiation, suggesting a protective role on stem cells.

Keywords: Nanoceria; stem cells; radiation; planarian.

Background

Ionizing radiation (IR) is indispensable in several applications including radiotherapy and medical imaging; however, it has several side effects, chiefly the production of massive DNA lesions. For example, a 2 Gray (Gy) dose of irradiation produced about 3000 DNA breaks per cell (1), including both single-strand (SSBs) and double-strand DNA (DSBs) breaks, While most of SSBs can be corrected, DSBs induce cell death. IR can directly induce DNA modifications, but also causes indirect effects by eliciting reactive oxygen species (ROS) production, such as hydrogen peroxide and superoxide anion radical, by water radiolysis (2). IR exposure triggers inflammatory responses, as irradiated cells produce inflammatory cytokines and growth factors (3), which promote the activity of ROS- and nitric oxide (NO)-producing enzymes such as cyclooxygenase-2 (COX-2), NADPH oxidase and NO synthase (4, 5). IR-mediated ROS overproduction, in turn, induces further DNA damage and cell death. The high extent of apoptosis overpowers the phagocytic system, inducing the activation of secondary necrosis with the release of cell components, such as heat shock proteins (HSP) and high-mobility group (HMG) box I (1).

One of the concerns about noxious IR effects is that the massive IR-induced DNA damage may cause tissue aging due to the depletion of stem cell compartment and consequently defects in the correct cell turnover and tissue homeostasis, although several mechanisms avoid the spread of DNA damages to stem cells and their progeny (6). For example, IR quickly induces senescence in neural stem cells and induce astrocytic differentiation (7), and irreparable DNA damage abolishes renewal of melanocyte stem cells in mice, which results in their premature differentiation (8). Overproduction of IR-induced ROS can be balanced by supplying non-enzymatic antioxidants such as tocopherol (vitamin E), carotene, carotenoids, retinol (vitamin A), ubiquinol, ascorbate (vitamin C) that, despite their proved protective activity, have a brief pharmacokinetic half-life, lack diffusion to site of the radical production and thus have to be constantly supplied.

Cerium oxide nanoparticles (nanoceria, NC) are a class of “nanozymes” that simulate the function of antioxidant enzymes, such as superoxide dismutase and catalase, due to the presence of crystalline defects on their surface that results in the presence of both Ce^{4+} and Ce^{3+} states (9). Due to their oxygen buffering capacity, NC can spontaneously self-regenerate to the initial Ce^{3+} state, making them an ideal inorganic antioxidant that exhibit self-regenerating capability, free-radical scavenging and anti-inflammatory activity, together with an excellent biocompatibility (10). Thus, NC are suitable for numerous biomedical applications (10), inhibiting adipogenesis (11) and providing protection in neurodegenerative (12) and cardiovascular diseases (13), in diabetes (14), in

psoriasis (15), in retinal damage (16), and in cancer (17). NC have also radioprotective effects as demonstrated in radiobiology studies on MRC-5 and MCF-7 cells, where NC exerts radioprotection on normal cells but not in cancer cells (18, 19). At the acidic pH of cancer microenvireonment, the catalase-mimicking activity of NC is inhibited, thus resulting in a sensitization of cancer cells to IR (20). Moreover, it has been demonstrated that NC have clinically relevance as protect mice lung from injuries induced by lethal dose of X-ray (21).

With the aim to investigate *in vivo* NC radioprotective effect on stem cells, we utilized planarians (Plathyelminthes), a model system for studying stem cells and tissue regeneration (22), biocompatibility and effects of nano- and micromaterials (23-28), as well as to perform pharmacological and toxicological assays (29,30).

Indeed, planarians possess an extraordinary tissue regeneration capability because they possess the neoblasts, a heterogeneous population of adult stem cells (31). After cutting, neoblasts started to proliferate and accumulate below the wound region producing a regenerative blastema (32), through which all missing body structures are eventually regenerated. Neoblast proliferation, commitment and differentiation can be followed in detail and genetically manipulated due to the availability of several molecular tools and cell-type specific markers, offering to the possibility to study and manipulate pluripotent stem cells *in vivo* and, concurrently, to study complex morphogenetic processes during tissue regeneration and organ formation. When planarians are treated with a high dose of X-rays, such as 30 Gy, neoblasts are selectively depleted and animals die (49). Interestingly, planarians treated with a low-dose of X-rays, such as 5 or 7 Gy, show an initial reduction in neoblast number that is then followed by the stimulation of massive neoblast division starting at the ventral side of animals (22, 50, 51). In this work, we analyzed the effect of NC in this depletion/repopulation process to prove the radioprotective effects of these nanoparticles on stem cells.

Methods

Animals

Planarians belonging to the species *Dugesia japonica*, asexual strain GI, were used in this work (49). Animals were maintained planarian water (52), and starved for 2 weeks before being used in the experiments. Authors state that all animals used were invertebrates and the experiments were performed in agreement with Italian law and EU Directive 2010/63/EU.

Nanoceria dispersion preparation and characterization

Nanoceria at 10 mg/ml (1406RE Nanoamor, Katy, TX) were dispersed through a mild sonication (GM mini20 Bandelin Sonopuls, Bandelin, Germany) in a gum Arabic (G9752 Sigma, Saint Louis, MO) 1 mg/ml solution in ultrapure MilliQ water (Millipore, Burlington, MA). Planarians were dipped for two days in a dispersion, which was obtained by diluting NC and gum Arabic (GA) in planarian water to 1 mg/ml and sonicating the mixture for 5 min at 8 W, using a probe sonicator (Fisherbrand Q125 Sonicator, Pittsburgh, PA). In all the experiments the control groups are animals treated with GA alone as it represents the vehicle in which nanoceria is dissolved, and since previous data demonstrate that this coating agent does not trigger modification in stem cell number as well as in planarian regeneration rate (23). Fresh dispersions were daily prepared. After treatment, planarians were thoroughly rinsed in planarian water to avoid external contamination by nanoparticles and then processed for experiments.

Bright field transmission electron microscopy (TEM) imaging and selected area electron diffraction (SAED) patterns of nanoceria were performed using a JEOL JEM-1011 microscope (JEOL Ltd., Tokyo, Japan) equipped with a tungsten thermionic gun operating at a 100 kV accelerating voltage. TEM images were acquired with a 11 Mp Orius 1000 CCD camera (Gatan, Pleasanton, CA).

In order to evaluate Ce(III) and Ce(IV) contents in nanoneria used in this work, X-ray photoelectron spectroscopy (XPS) analysis was carried out. A sample (1 mg of powder) was pressed to form a pellet and underwent analysis. Measurements were performed using a Kratos Axis UltraDLD spectrometer (Kratos Analytical Ltd., Manchester, UK) using a monochromatic Al Kα source ($h\nu$ = 1486.6 eV) operated at 20 mA and 15 kV. The analyses were carried out on a (300 × 700) μm^2 area. The high-resolution Ce 3d spectrum was collected at a pass-energy of 10 eV and an energy step of 0.1 eV. The Kratos charge neutralizer system was used during data acquisition. Data analysis was performed with CasaXPS software (Casa Software, Ltd., version 2.3.22).

Dynamic light scattering (DLS) and Z-potential investigation were performed using a Zeta-sizer NanoZS 90 (Malvern Instruments LTD, Malvern, UK). The measurements were carried out at 20°C in ultrapure water and in planarian water (NC concentration 50 μg/ml). The samples were sonicated for 1 min at 30% amplification using the probe sonicator to avoid the presence of aggregates before each reading. The hydrodynamic diameter and the Z-potential were evaluated as mean ± SD of 3 different measurements, with 15 runs for each of them. Finally, in order to assess mid-term stability of the prepared dispersions, hydrodynamic diameter and polydispersity index (PDI) were monitored at different time points (0, 30, 60, 90, 120 min) after the preparation.

Total Antioxidant Capacity Assay Kit (MAK187, Sigma, Saint Louis, MO) was used to evaluate the NC antioxidant efficacy; this kit exploit Cu^{2+} reduction to Cu^{+} ions due to the antioxidant sample, and a colorimetric probe reacts with Cu^{+}; the absorbance peak of colorimetric probe is thus proportionally correlated to the antioxidant ability of the sample. Briefly, NC were dispersed in ultrapure water at 0.1 mg/ml, 0.5 mg/ml and 1 mg/ml concentration, and Cu^{2+} working solution was added following the manufacturer's instruction. After 10 min of incubation at room temperature, the samples were centrifuged at 104 g for 15 minutes. Supernatants were collected and located in transparent 96 wells and absorbance read at 570 nm with a plate reader (VICTOR X3, Perkin Elmer, Waltham, MA). Standard curve of the antioxidant Trolox, a vitamin E analog, were obtained following the manufacturer's instruction, and antioxidant capacity of NC was expressed in terms of Trolox equivalence.

X-ray treatment

Intact planarians were uniformly exposed to the dose of 7 Gy (uncertainty of ± 2%), at the dose rate of 3 Gy/min, using a single 15MV beam of a linear accelerator for radiotherapy (Clinac DHX-S, Varian Medical Systems, Palo Alto, USA). The energy of the beam and the irradiation set-up was optimized to deliver a uniform radiation dose (± 2%) to the specimen.

Inductively-coupled plasma spectroscopy

Planarians treated with gum Arabic or NC were lyophilized and samples (40 mg) were processed for inductively coupled plasma spectroscopy. The pellets were digested with 1 ml of a HCl/HNO_3 solution (Carlo Erba super-pure grade, Milano, Italy) for 24 h. MilliQ grade water (18.3 MΩ) was then added (9 ml) to the samples, and cerium concentration was measured by means of elemental analysis (ICP-OES spectrometer, iCAP 6500, Thermo, Pittsburgh, PA). The 404.4 nm cerium emission line was used. Three independent experiments were performed.

Morphometric analysis of blastemal size

Two days after irradiation, control and NC-treated animals were cut between auricles and pharynx. Regenerating fragments were dipped after 3 days in 2% HCl for 5 min at 4°C, and then fixed in 100% ethanol (Sigma, Saint Louis, MO). Samples were analyzed under a Zeiss stereomicroscope (Stemi 305, Carl Zeiss Microscopy GmbH, Jena, Germany), and images were collected with a Zeiss camera (Axiocam Erc 5s, Carl Zeiss Microscopy GmbH, Jena, Germany). ImageJ software (53) was used to quantify digital images Blastema area was determined for 15 regenerating animals obtained from two independent experiments. The unpigmented region below the wound epithelium was

considered the blastema and the operator manually marked the blastemal margin. Data were analyzed by quantification of the ratio between blastema and body pieces areas.

Transmission electron microscopy on animals

TEM analysis of planarian was performed as previously described (38). Animals were fixed using 2.5% glutaraldehyde in 0.1 M cacodylate buffer and after two hours with 2% osmium tetroxide. Uranyl acetate and lead citrate were used to stain ultrathin sections and observation was performed with a JEOL 100 SX transmission electron microscope.

In situ hybridization on whole animals (WISH)

DNA templates for *DjMcm2* and *DjPiwi-A* were prepared as previously described (43, 49). Purified templates were *in vitro* transcribed using DIG-labeling mix (Roche Diagnostics GmbH, Mannheim, Germany) to obtain RNA probes labeled with DIG.

WISH was performed as previously described (28). Animals were processed for WISH 1, 2, or 3 days after X-ray treatment, time points at which a minimum number of stem cells is detectable (50). Animals were analyzed using a stereomicroscope and each animal was photographed at the same exposition and magnification; images were then changed into grayscale mode and inverted. The mean gray value (raw intensity/animal area) was then measured. Two independent experiments were performed.

Tunel assay

Tunel assay was carried out as described by Casella and colleagues (43) using the kit ApopTAg Red *in situ* apoptosis detection (EMD Millipore Corporation, Temecula, USA). Briefly, planarians were pre-treated with 2% HCl in 5/8 Holtfreter solution, fixed in 4% formaldehyde in PBST (PBS with 0.3% Triton X−100) and permeabilized in 1% SDS for 20 min. For staining, animals were incubated with terminal transferase enzyme for 4 h at 37°C, washed and then stained by using anti-digoxigenin-rhodamine-conjugated antibodies according to manufacturer's instruction (EMD Millipore Corporation, Temecula, USA). Stained animals were washed in PBST for 5 × 10 min, and analysed under a TCS SP8 confocal microscope (Leica Microsystems CMS, Mannheim, Germany). To record all Tunel-positive cells in each animal by means the 20x objective a 3D reconstruction was needed: tile scan acquisition mode assembled all adjoining microphotographic fields to form a single larger image of whole specimens in x/y dimension, zeta stack function recorded all plane in z-axis. Maximum projection of five planarians were analyzed for each experimental condition.

DNA comet assay

Alkaline Comet assay was applied for DNA damage analysis as previously described (23). Five planarians were used for each experimental point. Animals were gently homogenized, passed through a 30 μm filter spin column and centrifuged (300 g/min, 5 min at 4°C).
Slides were prepared in triplicates and ectrophoresis was performed for 7 min at a constant voltage of 1 V/cm (24 V, initial current 300 mA). The slides were then dipped in neutralizing solution, treated with 50 μL of SBYR® Gold nucleic acid gel stain (Thermofisher, Eugene, OR, USA) and examined for DNA damage.Samples were examined using a fluorescent microscope (Axioplan, Carl Zeiss Microscopy GmbH, Jena, Germany). One hundred and fifty cells *per* slide were analyzed. Analysis was performed as previously described (54). As reference, we used a standard scale of DNA damage that was prepared using diverse doses of X-ray on intact worms (54). The scoring scheme was based on a rank from 1 (no DNA damage: no tail) to 4 (high DNA damage: scattered tail).

Statistical analysis

The software GraphPad Prism 7.00 was used to perform statistical analysis.Statistical significance ($p < 0.05$) of data obtained from the experiments was evaluated with a Student's *t*-test for unpaired data.

Results

Characterization and uptake of NC in planarian

Figure 1 A shows a representative TEM image of the NC used in this work, while Figure 1 B depicts powder electron diffraction pattern, taken on areas of 10 μm in diameter, that show sharp diffraction rings indicating that the crystalline nature of the nanoparticles. The patterns can be indexed with a cubic face centered lattice.

Figure 1 C shows results of XPS analysis, *i.e.*, the binding energy region typical for Ce 3d peaks after background subtraction, together with the outcome of the fitting procedure. The best fit has been obtained with five sets of spin-orbit split doublets, three of which representative of Ce(IV) (green profiles in the figure) and two of Ce(III) (blue profiles) oxides, as described in the literature (55). The splitting between the two components of each doublet has been set to 18.6 eV (56), while the intensity ratio between the two components is set to 3:2, due to spin-orbit coupling. The relative concentration of Ce(III) and Ce(IV) species in the sample was calculated from the ratio of the

corresponding integrated areas of the XPS 3d peaks to the total integral area for the whole Ce 3d region. The acquired XPS spectrum is consistent with a Ce(III) percent concentration of 24.5 ± 1.0 % and a Ce(IV) percent concentration of 75.5 ± 1.0 %, corresponding to a Ce(III)/Ce(IV) ratio of about 0.3, that has been shown to be optimal for nanoceria antioxidant activities (57).

The stability of NC was evaluated with dynamic light scattering measurements. The average hydrodynamic diameter of NC is 516.3 ± 27.9 nm in ultrapure water and 612.3 ± 19.7 nm in planarian water, with a PDI of 0.49 ± 0.05 and of 0.47 ± 0.05, respectively. Z-potential measurements show a negative surface charge of -27.0 ± 0.3 mV and of -17.5 ± 0.5 mV for NC in ultrapure water and in planarian water, respectively. This shift of the Z-potential for the NC prepared in planarian water is due to the higher concentration of ions in the solvent, that partially screen the surface charge of the NC. The nanoceria dispersion mid-term stability was assessed as well in both ultrapure water and in planarian water over the time (0 - 120 min; Supporting Information). As depicted in Figure S1 A, average hydrodynamic diameter in both solutions do not significantly change over the time, as well as PDI (Figure S1 B), highlighting the excellent stability of the dispersions.

Antioxidant capacity of NC has been expressed in terms of equivalent of Trolox, as reported in Figure 1 D. The results demonstrate a linear correlation between NC concentration and its antioxidant ability (R^2 = 0.999), the antioxidant activity of 1 mg/ml of NC corresponding to the antioxidant activity of a Trolox solution of about 40 µM.

With the aim to understand NC effects on stem cells, we treated planarians with a dispersed nanoceria preparation. TEM images show the presence of NC aggregates inside cellular vacuoles (Figure 2 A). ICP analysis confirmed TEM data allowing the identification of a significant amount of cerium (Ce) in NC-treated planarians (121 ± 7 ng of Ce/mg of animal) with respect to the GA-treated animals (32 ± 15 ng of Ce/mg of animal; Figure 2 B).

Effect of NC on planarian stem cells and tissue regeneration in low-dose irradiated animals

To evaluate the effect of NC on neoblasts, we analyzed the expression of the neoblast cell-cycle related marker *DjMcm2* (49) and *DjPiwi-A* (58), the homolog of the cell cycle-unrelated stem cell marker *Smedwi-1* (34), *via* WISH, in NC- and GA-treated planarians exposed or not to 7 Gy early after irradiation 1 day after irradiation (Figure 3). *DjMcm2* and *DjPiwi-A* are expressed in both neoblasts spread in the parenchyma and clustered in dorso-lateral lines in GA- and NC-treated animals (Figure 3 B, C, G, H). Their expression is significantly reduced in GA- and NC-treated animals exposed to 7 Gy with respect to NC- and GA-treated animals not exposed to IR. Indeed,

DjMcm2- and *DjPiwi-A*-positive cells spread in the parenchyma are lost in these animals, and a few positive cells are only present in dorso-lateral clusters (Figure 3 D-F, I-K). However, in the presence of NC, a significantly higher hybridization signal is observable with respect to GA animals exposed to IR. A similar trend was observed 2 and 3 days after irradiation (data not shown).

Regeneration rate was evaluated by morphometric analysis of blastemal area in regenerating animals 3 days after cutting, as indicated in the scheme depicted in Figure 3 A. NC-treated animals exposed to low-dose of IR show a blastema area significantly higher than GA-treated animals exposed to the same dose of IR (Figure 3 L-P).

Effect of NC on cell death and DNA damage in low-dose irradiated animals

To further assay a possible protective effect of NC on low-dose irradiated planarians, we quantified apoptotic cell deaths by Tunel assay (Figure 4). Tunel-positive cells were distributed all over the planarian parenchyma in both GA- and NC-treated animals (Figure 4 A, B). As expected, we detected an activation of apoptosis in low-dose IR animals with respect to non-exposed animals (Figure 4 C, D, F). The number of Tunel-positive cells is significantly decreased in NC-treated animals exposed to IR with respect to GA-treated animals exposed to IR (C-F). As IR is known to induce DNA damage, we performed DNA comet assay (Figure 4 G-K). By classifying cell nuclei in four categories with progressive DNA damage, as depicted in examples of Figure 4 H-K, we found a substantial increase of nuclei with extremely damaged DNA (stage 4) and a reduction of nuclei with undamaged DNA (stage 1) in GA- and NC-treated animals exposed to IR respect to non-irradiated animals. However, by comparing NC- and GA-treated animals after low-dose irradiation, we observed a significant reduction of stage 4 nuclei and a significant increase of stage 1 nuclei in NC with respect to GA-treated animals (Figure 4 G).

Discussion

Localized IR induces damage to living cells, also in cells that are not directly irradiated because of their localization in distant tissues. It has been proposed that ROS prompted by IR-induced inflammation are responsible for the bystander effect that can be associated with several radiotherapy complications (1). NC, thanks to their self-renewing catalytic property as ROS scavengers, have been proposed for several biomedical applications (59).

In this work, we tested *in vivo* the protective effect of NC on IR-induced damage to stem cells using low-dose irradiated planarians as a model system. In planarians, neoblasts are the only dividing

cells; they exhibit dissimilar levels of radiosensitivity after low-dose of IR, with spread neoblasts that are less radioresistant than neoblasts clustered along the body. Therefore, spread neoblasts disappear within the first three days after IR and later radioresistant neoblasts start to proliferate and reconstitute the complex neoblasts system (50). Thus, low-dose irradiated planarians represent a good model that allows the monitoring of even slight variations in the number of stem cells and to investigate their effect on tissue regeneration.

With this aim, we treated animals with a non-toxic NC dose (23), and we found that NC were internalized inside planarian cells as previously demonstrated for NC and other nanoparticles (23, 25).

The expression levels of the S-phase marker *DjMcm2* (49) and the stem cell marker *DjPiwi-A* (58) were higher in NC-treated animals respect to GA-treated animals exposed to IR, indicating that neoblasts are preserved in NC-treated animals after low-dose of IR.

Neoblasts are involved in the blastema formation during regeneration (32), so we reasoned that NC-treated animals exposed to irradiation should produce a larger blastemal with respect to GA-treated animals, as NC-treated animals possessed a higher number of neoblasts. As expected, morphometric analysis showed that the blastema area value was higher in both regenerating tail and head of NC-treated animals with respect to GA-treated animals, corroborating the protective effect of NC on neoblasts. Accordingly, it has been demonstrated that NC stimulates regeneration *via* neoblastic activation in wild-type planarians, and it has been hypothesized that the antioxidant activity of NC can be the probable mechanism for the stimulation (25).

IR induces cell death and extensive DNA damage by ROS production (1). Radioprotective effect of NC against IR-genotoxicity has been well demonstrated *in vitro*, for example on human colon cells (60), on human lymphocytes (61), on human lung fibroblastic cells (MRC-5), and on breast cancer cells (MCF-7) (19). Some *in vivo* evidence of NC protective effects is also available, and a protection from IR-induced pneumonitis in athymic nude mice was demonstrated (62). Consistently, we found that NC significantly reduces IR-induced apoptosis in planarians, and that this correlates with a reduced occurrence of both DSB and SSB damage in NC-treated animals, owing to NC properties as ROS scavenger.

To the best of our knowledge, we demonstrate for the first time a radioprotective effect of NC on stem cells and in tissue regeneration *in vivo*. As fundamental molecular mechanisms and signaling pathways are conserved between higher vertebrates and planarians, we believe that our data represent a relevant step towards a translational application of NC in radiotherapy.

Funding

Our research did not receive any specific grant from funding agencies in the public, commercial, or not-for-profit sectors.

References

1. Najafi M, Motevaseli E, Shirazi A, Geraily G, Rezaeyan A, Norouzi F, et al. Mechanisms of inflammatory responses to radiation and normal tissues toxicity: clinical implications. *Int J Radiat Biol* 2018;**94**:335-56.

2. Lomax ME, Folkes LK, O'Neill P. Biological consequences of radiation-induced DNA damage: relevance to radiotherapy. *Clin Oncol (R Coll Radiol)* 2013;**25**:578-85.

3. Siva S, MacManus M, Kron T, Best N, Smith J, Lobachevsky P, et al. A pattern of early radiation-induced inflammatory cytokine expression is associated with lung toxicity in patients with non-small cell lung cancer. *PLoS One* 2014;**9**:e109560.

4. Marozik P, Mothersill C, Seymour CB, Mosse I, Melnov S. Bystander effects induced by serum from survivors of the Chernobyl accident. *Exp Hematol* 2007;**1**:55-63.

5. Fardid R, Najafi M, Salajegheh A, Kazemi E, Rezaeyan A. Radiation-induced non-targeted effect *in vivo*: Evaluation of cyclooygenase-2 and endothelin-1 gene expression in rat heart tissues. *J Cancer Res Ther* 2017;13:51-5.

6. Vitale I, Manic G, De Maria R, Kroemer G, Galluzzi L. DNA damage in stem cells. *Mol Cell* 2017; **66**:306-19.

7. Schneider L, Pellegatta S, Favaro R, Pisati F, Roncaglia P, Testa G, et al. DNA damage in mammalian neural stem cells leads to astrocytic differentiation mediated by BMP2 signaling through JAK-STAT. *Stem Cell Reports* 2013;**1**:123-38.

8. Inomata K, Aoto T, Binh NT, Okamoto N, Tanimura S, Wakayama T, et al. Genotoxic stress abrogates renewal of melanocyte stem cells by triggering their differentiation. *Cell* 2009;**137**:1088-99.

9. Chen BH, Stephen Inbaraj B. Various physicochemical and surface properties controlling the bioactivity of cerium oxide nanoparticles. *Crit Rev Biotechnol* 2018;**38**:1003-24.

10. Das S, Dowding JM, Klump KE, McGinnis JF, Self W, Seal S. Cerium oxide nanoparticles: applications and prospects in nanomedicine. *Nanomedicine* 2013;**8**:1483-508.

11. Rocca A, Mattoli V, Mazzolai B, Ciofani G. Cerium oxide nanoparticles inhibit adipogenesis in rat mesenchymal stem cells: potential therapeutic implications. *Pharm Res* 2014;**31**:2952-62.

12. Rzigalinski BA, Carfagna CS, Ehrich M. Cerium oxide nanoparticles in neuroprotection and considerations for efficacy and safety. *Wiley Interdiscip Rev Nanomed Nanobiotechnol* 2017;**9**:4.

13. Niu J, Azfer A, Rogers LM, Wang X, Kolattukudy PE. Cardioprotective effects of cerium oxide nanoparticles in a transgenic murine model of cardiomyopathy. *Cardiovasc Res* 2007;73:549-59.

14. Pourkhalili N, Hosseini A, Nili-Ahmadabadi A, Hassani S, Pakzad M, Baeeri M, et al. Biochemical and cellular evidence of the benefit of a combination of cerium oxide nanoparticles and selenium to diabetic rats. *World J Diabetes* 2011;**2**:204-10.

15. Domala A, Bale S, Godugu C. Protective effects of nanoceria in imiquimod induced psoriasis by inhibiting the inflammatory responses. *Nanomedicine* 2020;**15**:5-22.

16. Zhou X, Wong LL, Karakoti AS, Seal S, McGinnis JF. Nanoceria inhibit the development and promote the regression of pathologic retinal neovascularization in the Vldlr knockout mouse. *PLoS One* 2011;6:e16733.

17. Martinelli C, Pucci C, Ciofani G. Nanostructured carriers as innovative tools for cancer diagnosis and therapy. *APL Bioeng* 2019;**3**:011502.

18. Ouyang Z, Mainali MK, Sinha N, Strack G, Altundal Y, Hao Y, et al. Potential of using cerium oxide nanoparticles for protecting healthy tissue during accelerated partial breast irradiation (APBI). *Phys Med* 2016;**32**:631-5.

19. Abdi Goushbolagh N, Abedi Firouzjah R, Ebrahimnejad Gorji K, Khosravanipour M, Moradi S, Banaei A, et al. Estimation of radiation dose-reduction factor for cerium oxide nanoparticles in MRC-5 human lung fibroblastic cells and MCF-7 breast-cancer cells. *Artif Cells Nanomed Biotechnol* 2018;**46**:S1215-25.

20. Wason MS, Colon J, Das S, Seal S, Turkson J, Zhao J, et al. Sensitization of pancreatic cancer cells to radiation by cerium oxide nanoparticle-induced ROS production. *Nanomedicine* 2013;**9**:558-69

21. Xu PT, Maidment BW 3rd, Antonic V, Jackson IL, Das S, Zodda A, et al. Cerium Oxide Nanoparticles: a potential medical countermeasure to mitigate radiation-nduced Lung Injury in CBA/J Mice. *Radiat Res* 2016;185:516-26.

22. Rossi L, Salvetti A. Planarian stem cell niche, the challenge for understanding tissue regeneration. *Semin Cell Dev Biol* 2019;**87**:30-6.

23. Salvetti A, Rossi L, Iacopetti P, Li X, Nitti S, Pellegrino T, et al. *In vivo* biocompatibility of boron nitride nanotubes: effects on stem cell biology and tissue regeneration in planarians. *Nanomedicine* 2015;**10**:1911-22.

24. Kazan A, Yesil-Celiktas O, Zhang YS. Fabrication of Thymoquinone-Loaded Albumin Nanoparticles by Microfluidic Particle Synthesis and Their Effect on Planarian Regeneration. *Macromol Biosci* 2019;**19**:e1900182.

25. Ermakov A, Popov A, Ermakova O, Ivanova O, Baranchikov A, Kamenskikh K, et al. The first inorganic mitogens: Cerium oxide and cerium fluoride nanoparticles stimulate planarian regeneration via neoblastic activation. *Mater Sci Eng C Mater Biol Appl* 2019;**104**:109924.

26. Tran TA, Hesler M, Moriones OH, Jimeno-Romero A, Fischer B, Bastús NG, et al. Assessment of iron oxide nanoparticle ecotoxicity on regeneration and homeostasis in the replacement model system Schmidtea mediterranea. *Altex* 2019;**36**:583-96.

27. Leynen N, Van Belleghem FGAJ, Wouters A, Bove H, Ploem JP, Thijssen E, et al. *In vivo* Toxicity Assessment of Silver Nanoparticles in Homeostatic versus Regenerating Planarians. *Nanotoxicology* 2019;**13**:476-91.

28. Gambino G, Falleni A, Nigro M, Salvetti A, Cecchettini A, Ippolito C, et al. Dynamics of interaction and effects of microplastics on planarian tissue regeneration and cellular homeostasis. *Aquat Toxicol* 2020;**218**:105354.

29. Zhang S, Hagstrom D, Hayes P, Graham A, Collins ES. Multi-behavioral endpoint testing of an 87-chemical compound library in freshwater planarians. *Toxicol Sci* 2019;167:26-44.

30. Wu JP, Li MH. The use of freshwater planarians in environmental toxicology studies: Advantages and potential. *Ecotoxicol Environ Saf* 2018;**161**:45-56.

31. Alessandra S, Rossi L. Planarian Stem Cell Heterogeneity. *Adv Exp Med Biol* 2019;**1123**:39-54.

32. Rossi L, Salvetti A, Batistoni R, Deri P, Gremigni V. Planarians, a tale of stem cells. *Cell Mol Life Sci* 2008;**65**:16-23.

33. Salvetti A, Lena A, Rossi L, Deri P, Cecchettini A, Batistoni R, Gremigni V. Characterization of DeY1, a novel Y-box gene specifically expressed in differentiating male germ cells of planarians. *Gene Expr Patterns* 2002;**2**:195-200.

34. Reddien PW, Oviedo NJ, Jennings J, Renkin JC, Sánchez Alvarado A. SMEDWI-2 is a PIWI-like protein that regulates planarian stem cells. *Science* 2005;**310**:1327–130.

35. Salvetti A, Rossi L, Lena A, Batistoni R, Deri P, Rainaldi G, et al. DjPum, a homologue of Drosophila Pumilio, is essential to planarian stem cell maintenance. *Development* 2005;**132**:1863-74.

36. Rossi L, Salvetti A, Lena A, Batistoni R, Deri P, Pugliesi C, et al. DjPiwi-1, a member of the PAZ-Piwi gene family, defines a subpopulation of planarian stem cells. *Dev Genes Evol* 2006;**216**:335-46.

37. Rossi L, Salvetti A, Marincola FM, Lena A, Deri P, Mannini L, et al. Deciphering the molecular machinery of stem cells: a look at the neoblast gene expression profile. *Genome Biol* 2007;**8**:R62.

38. Bonuccelli L, Rossi L, Lena A, Scarcelli V, Rainaldi G, Evangelista M, et al. An RbAp48-like gene regulates adult stem cells in planarians. *J Cell Sci* 2010;**123**:690-8.

39. Peiris TH, Weckerle F, Ozamoto E, Ramirez D, Davidian D, García-Ojeda ME, et al. TOR signaling regulates planarian stem cells and controls localized and organismal growth. *J Cell Sci* 2012;125:1657-65.

40. van Wolfswinkel JC, Wagner DE, Reddien PW. Single-cell analysis reveals functionally distinct classes within the planarian stem cell compartment. *Cell Stem Cell* 2014;**15**:326-39.

41. Rossi L, Bonuccelli L, Iacopetti P, Evangelista M, Ghezzani C, Tana L, et al. Prohibitin 2 regulates cell proliferation and mitochondrial cristae morphogenesis in planarian stem cells. *Stem Cell Rev Rep* 2014;**10**:871-87.

42. Rodríguez-Esteban G, González-Sastre A, Rojo-Laguna JI, Saló E, Abril JF. Digital gene expression approach over multiple RNA-Seq data sets to detect neoblast transcriptional changes in Schmidtea mediterranea. *BMC Genomics* 2015;**16**:361.

43. Cassella L, Salvetti A, Iacopetti P, Ippolito C, Ghezzani C, Gimenez G, et al. Putrescine independent wound response phenotype is produced by ODC-like RNAi in planarians. *Sci Rep* 2017;**7**: 9736-53.

44. Zeng A, Li H, Guo L, Gao X, McKinney S, Wang Y, et al. Prospectively isolated tetraspanin(+) neoblasts are adult pluripotent stem cells underlying planaria regeneration. *Cell* 2018;173:1593-1608.

45. Krishna S, Palakodeti D, Solana J. Post-transcriptional regulation in planarian stem cells. *Semin Cell Dev Biol* 2019;**87**:69-78.

46. Thiruvalluvan M, Barghouth PG, Tsur A, Broday L, Oviedo NJ. SUMOylation controls stem cell proliferation and regional cell death through Hedgehog signaling in planarians. *Cell Mol Life Sci* 2018;**75**:1285-1301

47. Plass M, Solana J, Wolf FA, Ayoub S, Misios A, Glažar P, et al. Cell type atlas and lineage tree of a whole complex animal by single-cell transcriptomics. *Science* 2018;**360**:eaaq1723.

48. Fincher CT, Wurtzel O, de Hoog T, Kravarik KM, Reddien PW. Cell type transcriptome atlas for the planarian Schmidtea mediterranea. *Science* 2018;**360**:eaaq1736.

49. Salvetti A, Rossi L, Deri P, Batistoni R. An MCM2-related gene is expressed in proliferating cells of intact and regenerating planarians. *Dev Dyn* 2000;**218**:603-14.

50. Salvetti A, Rossi L, Bonuccelli L, Lena A, Pugliesi C, Rainaldi G, et al. Adult stem cell plasticity: neoblast repopulation in non-lethally irradiated planarians. *Dev Biol* 2009;**328**:305-14.

51. Rossi L, Cassella L, Iacopetti P, Ghezzani C, Tana L, Gimenez G, et al. Insight into stem cell regulation from sub-lethally irradiated worms. *Gene* 2018;**662**:37-45.

52. Degl'Innocenti A, Rossi L, Salvetti A, Marino A, Meloni G, Mazzolai B, et al. Chlorophyll derivatives enhance invertebrate red-light and ultraviolet phototaxis. *Sci Rep* 2017;**7**:3374.

53. Abramoff MD, Magelhaes PJ, Ram SJ. Image processing with ImageJ. *Biophot* 2004;**11**:36-42.

54. Peiris TH, Ramirez D, Barghouth PG, Ofoha U, Davidian D, Weckerle F, Oviedo NJ. Regional signals in the planarian body guide stem cell fate in the presence of genomic instability. *Development* 2016;**143**:1697-709.

55. Zhou J, Perket JM, Zhou J. Growth of Pt Nanoparticles on reducible CeO_2(111) thin films: effect of nanostructures and redox properties of ceria. *J. Phys. Chem. C* 2010; **114**:11853-11860.

56. Bêche E, Charvin P, Perarnau D, Abanades S, Flamant G. Ce 3d XPS investigation of cerium oxides and mixed cerium oxide ($Ce_xTi_yO_z$). *Surf. Interface Anal.* 2008; **40**: 264–267.

57. Celardo I, De Nicola M, Mandoli C, Pedersen JZ, Traversa E, Ghibelli L. Ce^{3+} ions determine redox-dependent anti-apoptotic effect of cerium oxide nanoparticles. *ACS Nano.* 2011; **5**:4537–4549.

58. Yoshida-Kashikawa M, Shibata N, Takechi K, Agata K. DjCBC-1, a conserved DEAD box RNA helicase of the RCK/p54/ Me31B family, is a component of RNA-protein complexes in planarian stem cells and neurons. *Dev Dyn* 2007;236:3436-50.

59. Pezzini I, Marino A, Del Turco S, Nesti C, Doccini S, Cappello V, et al. Cerium oxide nanoparticles: the regenerative redox machine in bioenergetic imbalance. *Nanomedicine* 2017;**12**:403-16.

60. Colon J, Hsieh N, Ferguson A, Kupelian P, Seal S, Jenkins DW, et al. Cerium oxide nanoparticles protect gastrointestinal epithelium from radiation-induced damage by reduction of reactive oxygen species and upregulation of superoxide dismutase 2. *Nanomedicine* 2010;**6**:698-705.

61. Zal Z, Ghasemi A, Azizi S, Asgarian-Omran H, Montazeri A, Hosseinimehr SJ. Radioprotective effect of cerium oxide nanoparticles against genotoxicity induced by ionizing radiation on human lymphocytes. *Curr Radiopharm* 2018;11:109-115.

62. Colon J, Herrera L, Smith J, Patil S, Komanski C, Kupelian P, et al. Protection from radiation-induced pneumonitis using cerium oxide nanoparticles. *Nanomedicine* 2009;**5**:225-31.

Figure captions

Figure 1 Nanoceria characterization. A**)** TEM bright field representative image. B) Powder electron diffraction pattern, showing the crystalline structure of the nanoparticles. C) XPS analysis, showing a Ce(III)/Ce(IV) ratio of about 0.3. D) Evaluation of antioxidant capacity.

Figure 2 Analysis of NC internalization. A) TEM image depicting a detail of a cell cytoplasm portion showing nanoparticles (harrowheads) inside two vacuoles, observed in ultrathin section from a NC treated planarian. Scale bar is 5 μm. B) Graph indicating Ce amount in NC-treated planarians as assessed by elemental analysis. Each column bar is the mean value ± standard deviation of three independent experiments. Significant differences were evaluated by unpaired student *t*-test analysis (** $p < 0.01$).

Figure 3 *DjMcm* and *DjPiwi-A* expression and morphometric analysis of head and tail blastema in low-dose exposed animals pre-treated with NC or GA, as a control. A) Schematic representation of the experimental setup. Numbers indicate the day. B) Representative image of *DjMcm2* expression in a GA-treated animal. C) Representative image of *DjMcm2* expression in a NC-treated animal. D) Representative image of *DjMcm2* expression in a GA-treated animal exposed to X-rays. E) Representative image of *DjMcm2* expression in a NC-treated animal exposed to X-rays. Scale bar is 500 μm. F) Quantification of signal intensity detected by WISH in GA-treated planarians (GA), NC-treated planarians (NC), GA-treated planarians exposed to X-rays (GA 7 Gy) and NC-treated planarians exposed to X-rays (NC 7 Gy). Each column bar is the mean value ± standard deviation of mean gray values measured in at least 10 animals. Significant differences were evaluated by unpaired student *t*-test analysis (**** $p < 0.0001$; ns not significant). G) Representative image of *DjPiwi-A* expression in a GA-treated animal. H) Representative image of *DjPiwi-A* expression in a NC-treated animal. I) Representative image of *DjPiwi-A* expression in a GA-treated animal exposed to X-rays. J) Representative image of *DjPiwi-A* expression in a NC-treated animal exposed to X-rays. Scale bar corresponds to 500 μm. K) Quantification of signal intensity detected by WISH in GA-treated planarians (GA), NC-treated planarians (NC), GA-treated planarians exposed to X-rays (GA 7 Gy) and NC-treated planarians exposed to X-rays (NC 7 Gy). Each column bar is the mean value ± standard deviation of mean gray values measured in at least 10 animals. Significant differences were evaluated by unpaired student *t*-test analysis (**** $p < 0.0001$; *** $p < 0.001$; * $p < 0.05$; ns not significant). L) Representative image of a GA-treated planarian fragment

regenerating a new head after 7 Gy exposure. M) Representative image of a NC-treated planarian fragment regenerating a new head after 7 Gy exposure. N) Representative image of a GA-treated planarian fragment regenerating a new tail after 7 Gy exposure. O) Representative image of a NC-treated planarian fragment regenerating a new tail after 7 Gy exposure. Blastemal regions are indicated by a harrowhead. Scale bar is 500 μm. P) Morphometric analysis of blastema. Each column bar is the mean ± standard deviation of two independent experiments (each including 15 different specimens). Significant differences were evaluated by unpaired student *t*-test analysis (* $p < 0.05$).

Figure 4. Analysis of cell death and DNA damage in low-dose exposed animals pretreated with NC or GA. Representative confocal images of Tunel assay performed in A) GA-treated planarians, B) NC-treated planarians, C) GA-treated planarians exposed to X-rays, D) NC-treated planarians exposed to X-rays. Tunel-positive cells are visualized as red dots. Scale bar is 500 μm in A-D. E) Schematic representation of the experimental setup. Numbers indicate the days. F) Quantification of Tunel-positive cells (number of positive cells/animal area). Each column bar is the mean value ± standard deviation of values from at least 4 animals. Significant differences were evaluated by unpaired student *t*-test analysis (*** $p < 0.001$; * $p < 0.05$). G) Percentage of cells with different levels of DNA damage in GA-treated planarians (GA), NC-treated planarians (NC), GA-treated planarians exposed to X-rays (GA 7 Gy) and NC-treated planarians exposed to X-rays (NC 7 Gy). Each column bar represents the mean value ± standard deviation of three independent experiments. Significant differences were evaluated by unpaired student *t*-test analysis (*$p < 0.05$). H) Representative image of a nucleus showing no DNA damage (1). I-K) Representative images of nuclei showing low (2), moderate (3) and high (4) DNA damage. Scale bar: 10 μm.

Figure 1

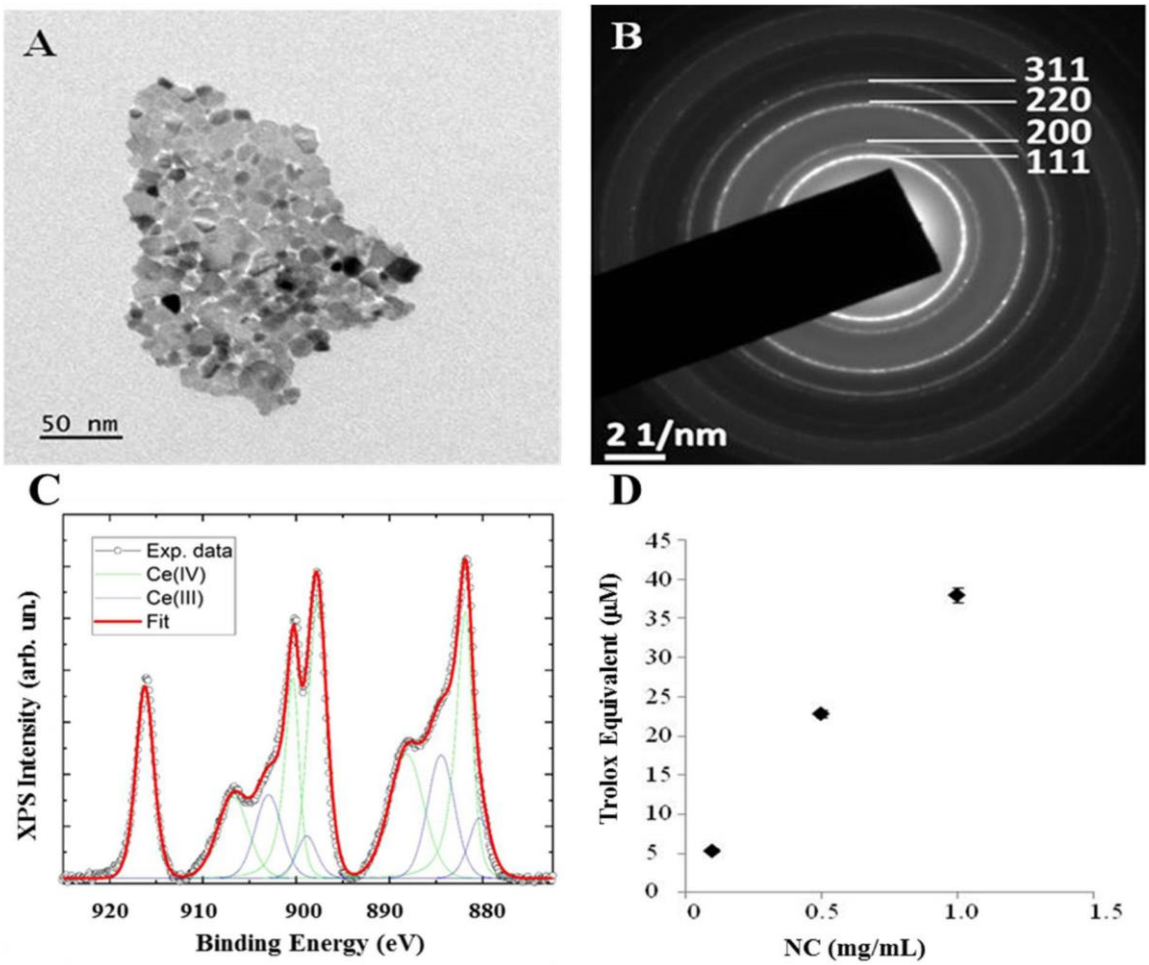
A
50 nm
B
311
220
200
111
2 1/nm
C
Exp. data
Ce(IV)
Ce(III)
Fit
XPS Intensity (arb. un.)
920
910
900
890
880
Binding Energy (eV)
D
Trolox Equivalent (μM)
45
40
35
30
25
20
15
10
5
0
0
0.5
1.0
1.5
NC (mg/mL)

Figure 2

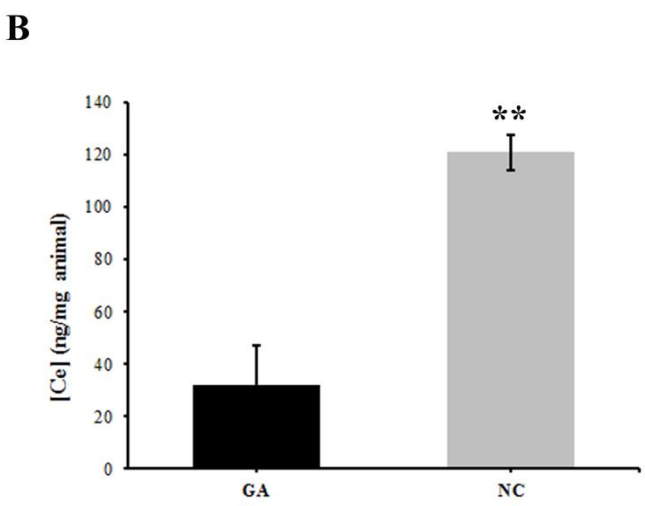

Figure 3

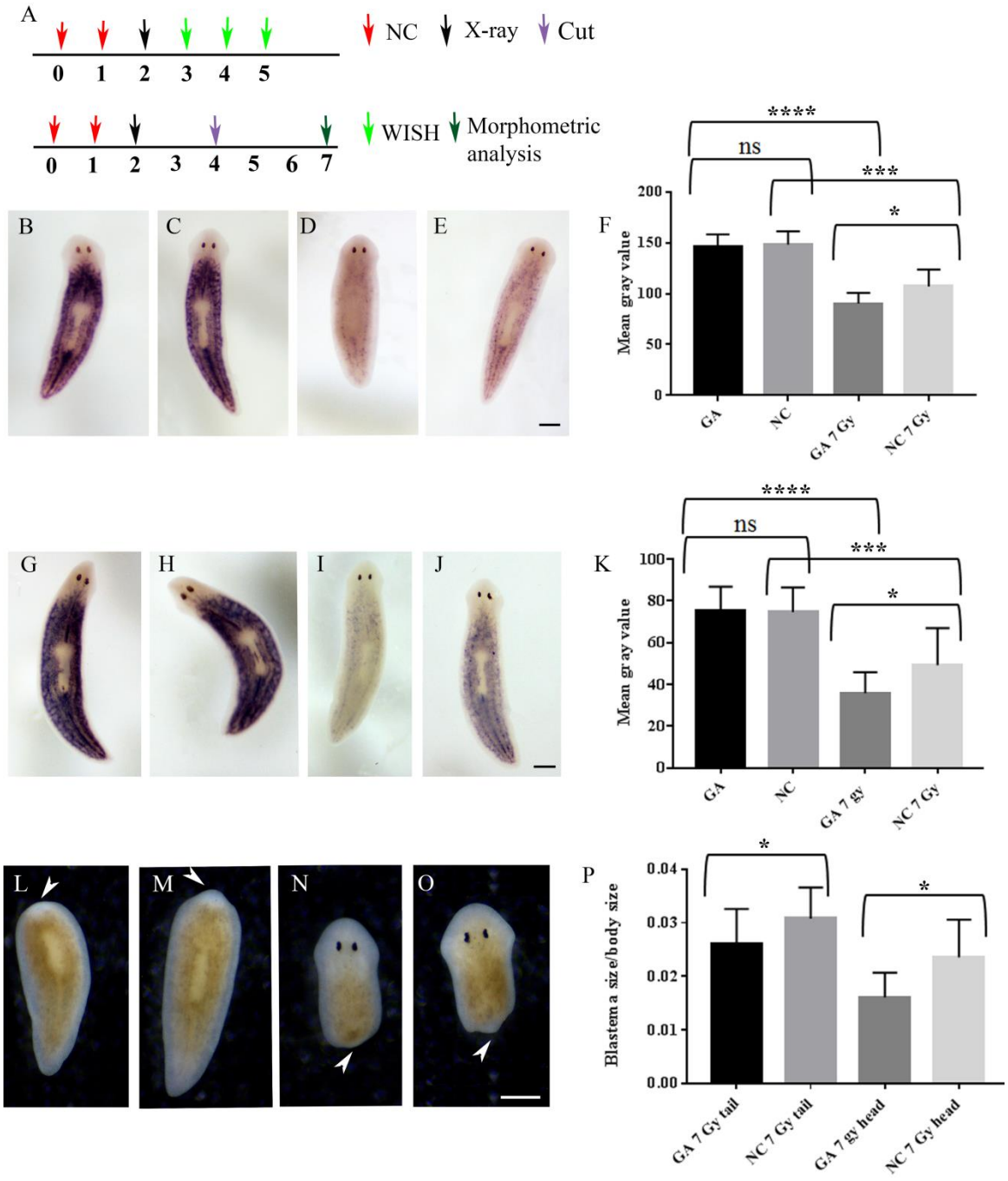
A
NC
X-ray
Cut
0 1 2 3 4 5
WISH
Morphometric analysis
0 1 2 3 4 5 6 7
B
C
D
E
F
Mean gray value
GA
NC
GA 7 Gy
NC 7 Gy
ns
***
*
G
H
I
J
K
Mean gray value
GA
NC
GA 7 gy
NC 7 Gy
L
M
N
O
P
Blastema size/body size
GA 7 Gy tail
NC 7 Gy tail
GA 7 gy head
NC 7 Gy head

Figure 4

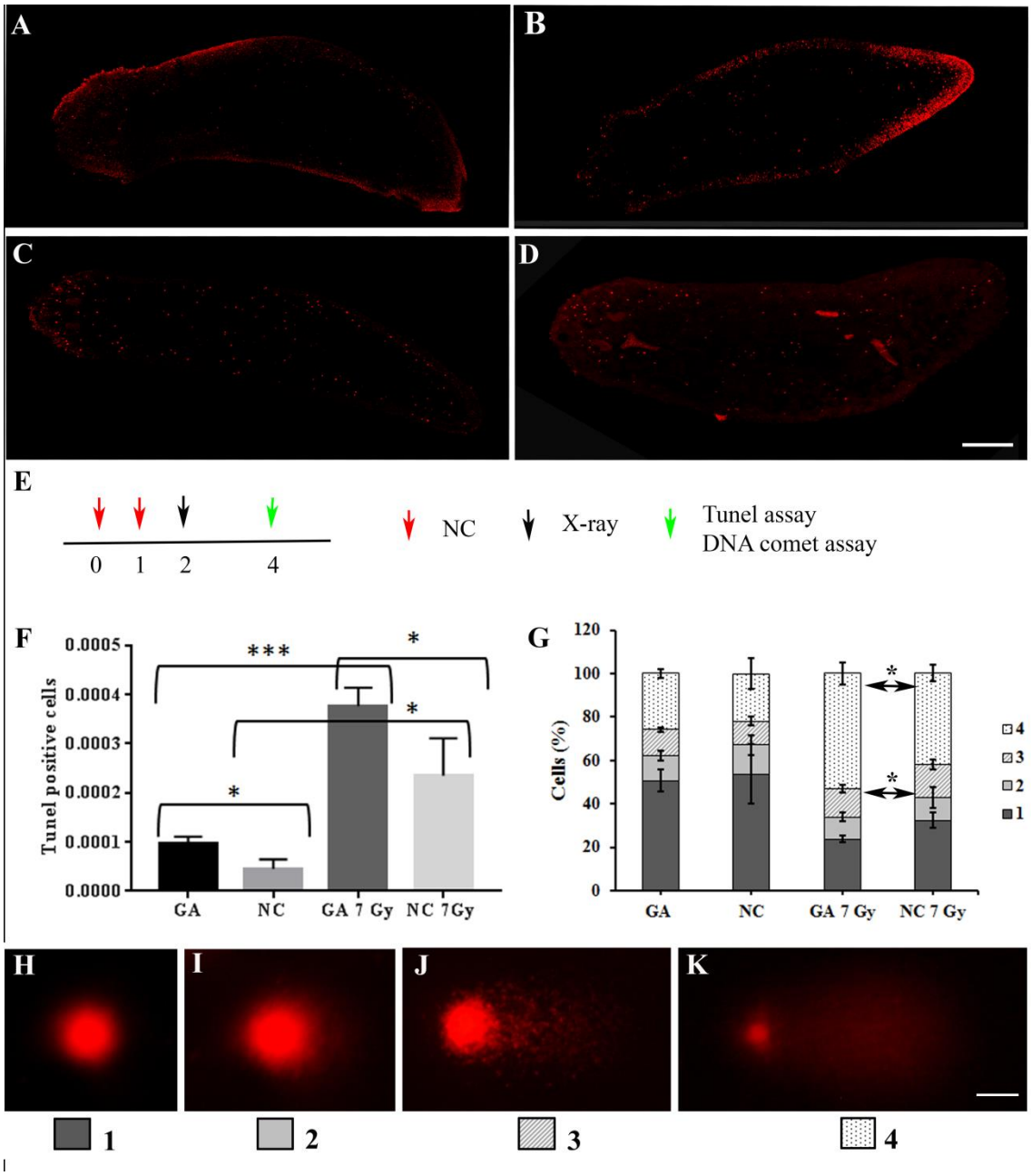
A
B
C
D
E
0 1 2 4
NC
X-ray
Tunel assay
DNA comet assay
F
Tunel positive cells
0.0005
0.0004
0.0003
0.0002
0.0001
0.0000
***
*
*
*
GA
NC
GA 7 Gy
NC 7Gy
G
Cells (%)
120
100
80
60
40
20
0
*
*
4
3
2
1
GA
NC
GA 7 Gy
NC 7 Gy
H
I
J
K
1
2
3
4